Virology Journal

RESEARCH

Open Access

Identification of Co-29, a 5-cyano-2-thiacetyl aromatic pyrimidinone, as a potential inhibitor targeting the RdRp of norovirus

Xianglan Liu[1†], Jiaming Hu[1,3†], Jiarui Wu[2†], Yiru Tian[1,4], Jinbo Wang[2], Chunyan Wu[1], Qingfeng Chen[1], Leonard Krall[1], Yanping He[2*] and Qun Lu[1*]

Abstract

Background Human norovirus (HNV) is the predominant pathogen causing outbreaks of acute gastroenteritis globally. Despite significant efforts to combat norovirus infections, there is currently no FDA approved vaccine or antiviral drug available. Consequently, the development of effective antiviral agents is of critical importance.

Methods and results In this study, a series of 41 5-cyano-2-thiacetyl aromatic pyrimidinone compounds were designed and synthesized. A cell viability-based screening for anti-murine norovirus (MNV) compounds was conducted, revealing that compound 29 (hereafter used as Co-29) exhibited antiviral activity against MNV. Co-29 demonstrated effective inhibition of MNV^{CW3} RNA replication, exhibiting an EC_{50} of 58.22 μM. An RdRp enzyme activity assay indicated that Co-29 directly inhibits RdRp activity to both MNV and HNV. Molecular docking studies suggested that Co-29 interacts with the palm region of RdRp via hydrogen bonding with specific residues, which are conserved in RdRps across MNV and HNV norovirus variants.

Conclusions In conclusion, our study suggests that the newly synthesized Co-29 may serve as a potential antiviral candidate or lead compound for future studies.

Keywords Norovirus, RdRp, Anti-norovirus agent, Co-29

[†]Xianglan Liu, Jiaming Hu and Jiarui Wu have contributed equally to this work.

*Correspondence:
Yanping He
yphe@ynu.edu.cn
Qun Lu
qunlu@ynu.edu.cn
[1] Center for Life Sciences, School of Life Sciences, Yunnan Key Laboratory of Cell Metabolism and Diseases, Yunnan University, Kunming, Yunnan, China
[2] Key Laboratory of Medicinal Chemistry for Natural Resource, Yunnan Provincial Center for Research and Development of Natural Products, Ministry of Education, School of Pharmacy, Yunnan University, Kunming, Yunnan, China
[3] School of Life Sciences, Southern University of Science and Technology, Shenzhen, Guangdong, China
[4] Laboratory of Molecular Immunology, Institute of Medical Biology, Chinese Academy of Medical Sciences& Peking Union Medical College, Kunming, Yunnan, China

Background

Norovirus, often referred to as the "winter vomiting bug", is a highly contagious virus that causes gastroenteritis, an inflammation of the stomach and intestines. Infection is accompanied with representative symptoms including the sudden onset of severe vomiting, diarrhoea, and abdominal pain, often accompanied by fever and headache. It accounts for approximately 20% of the global burden of acute gastroenteritis worldwide, and is responsible for outbreaks in crowded environments, including schools, cruise lines, and healthcare facilities, which leads to an estimated $60 billion loss annually [1–4]. In the United States, during the first week of December 2024, 91 separate outbreaks of norovirus occurred [4]. Human norovirus (HNV) spreads through contaminated food, water, surfaces, and direct contact with infected individuals, causing roughly 685 million infections and 200,000 deaths annually, with 70,000 or more among children in developing countries [5, 6]. Due to its ability to spread rapidly and its resilience in various environments, there is a pressing need for effective antiviral treatments. However, there have been no approved vaccines or treatments to date, due to the characteristics of the virus, as it possesses a high genetic variability and rapid evolution [3, 7, 8].

Norovirus, belonging to the *Caliciviridae* family, is a nonenveloped positive-sense, single-stranded (+ssRNA) virus, with a 7.4–7.7-kb genome encoding three open reading frames (ORFs) [9, 10]. ORF2 and ORF3 encode the major (VP1) and minor (VP2) capsid proteins to form the viral particle [11, 12]. Based on the amino acid sequences of VP1, norovirus can be classified into 10 genogroups, GI to GX. Among them, GI, GII, GIV, GVIII, and GIX are known to be able to infect humans [10]. ORF1 encodes a polyprotein precursor that generates nonstructural proteins following proteolytic cleavage, including an RNA-dependent RNA polymerase (RdRp) and other factors which are essential for viral gene expression and replication [9, 13].

As the critical enzyme for viral genome synthesis, RdRp is highly conserved among RNA viruses which makes it a highly attractive target for antiviral research [14]. The structure of HNV RdRp resembles a closed right hand, with thumb, fingers, and palm domains, as well as an N-terminal domain linking the fingers and thumb [15–17]. There are two major classes of RdRp-targeting antiviral agents: the nucleoside analogs (NAs) and the non-nucleoside inhibitors (NNIs). NAs bind in the RdRp active site, which is situated within the palm domain, through mimicry of incoming nucleoside triphosphates (NTPs) to inhibit RNA synthesis [18]. 2′-C-methyl-cytidine (2CMC), a popular cytidine analogue which has been widely reported as a potential anti-norovirus NA, is limited by its safety and efficacy [19–22]. NNIs provide an alternative strategy for the development of anti-norovirus drugs. They exhibit their antiviral activity through binding to allosteric sites in the RdRp and blocking its conformational rearrangement, which is required to form the active replication complex [23, 24]. Two binding sites for NNIs in HNV RdRp have been identified, site A and site B. Site A is located between the fingers and thumb domains, functioning as a positively charged NTP traversal channel with flexible amino acid side chains. Site B is a highly conserved allosteric binding pocket within the thumb region which forms a cleft along the newly synthesized RNA exit path, which is a highly conserved allosteric binding pocket within the thumb region [25–27]. Suramin and its derivative NF023 are effective to inhibit HNV and murine norovirus (MNV) by binding to Site A [25]. PPNDS and NAF2, two Suramin derivatives, bind into both Site A and Site B to inhibit the enzyme activity [26, 28, 29]. A high-throughput virtual screening was performed to identify ligands binding to Site B of HNV and MNV RdRps, and two candidates, compound 11 and 54 were selected with low IC_{50} values, however they were ineffective against MNV in cell culture [30]. A recent study also applied a structure-based virtual screening specifically targeting Site B of HNV RdRp and found a hydrochloride hydrate, CX-6258, as a general inhibitor of norovirus RdRp [31]. Furthermore, based on the sequence conservation of RdRp among RNA viruses, a group evaluated the antiviral activity of hepatitis C virus (HCV) NNIs against HNV RdRp. From this study, JKT-109 was identified with broad-spectrum antiviral activity across several genera of *Caliciviridae* [28]. While a growing number of researchers have been working on anti-norovirus drug identification, currently all drug candidates are still limited by the challenges of low bioavailability and the presence of nonspecific off-target effects [32–34]. Therefore, the discovery of new anti-norovirus compounds is still urgently needed.

A synthesized compound, 7a'k, has been shown inhibit dengue virus (DENV) RdRp enzyme activity [35]. In this study, using a similar design strategy, we first synthesized 41 new compounds using the molecular hybridization method with 3jc, a HCV RdRp inhibitor [36], and 4w, a Zika virus (ZIKV) RdRp inhibitor [37] as the lead compounds. 4w and 3jc are both 2,5,6-trisubstituted pyrimidinone derivatives, which exhibit certain structural similarities and act on the conserved NS5 RdRp enzyme in flaviviruses. We constructed the target compound's structure by retaining the pyrimidinone core and combining the *C*−2 thioacetyl phenyl amine side chain from 4w, along with the *C*−6 substituted phenyl ring and a *C*−5 cyano group from 3jc. Various substituents were introduced at the R_1, and R_2 position to increase structural

diversity. As a result, a series of 41 novel 5-cyano-2-thioacetyl phenylamine pyrimidinone target compounds has been designed and synthesized (Fig. 1). We then screened for a high ratio of live cells after MNV infection with anti-MNV compounds. One of them, Co-29, exhibited in vitro antiviral activity to MNV. Co-29 efficiently inhibited the MNV^{CW3} RNA replication with an EC_{50} of 58.22 μM. An RdRp enzyme activity assay showed that Co-29 directly inhibited the activity of RdRp for both MNV (IC^{50} = 32.04 μM) and HNV (IC^{50} = 36.62 μM). Molecular docking predicted that Co-29 binds to the palm region of RdRp through hydrogen bonding with residues which are conserved in RdRps across norovirus variants including MNV and HNV.

Methods

Chemical compounds and synthesis

According to the procedure described previously [35], the synthesis route of the target compounds is depicted in Scheme 1. The specific synthesis procedure is described as below. (I) Synthesis of 2-bromoacetanilide derivatives (3a-g): Aniline derivatives **1a-g** (10 mmol, 1 equiv) and anhydrous TEA (15 mmol, 1.5 equiv) were put into a round bottom flask and the solvent anhydrous CH_2Cl_2 (150 mL) was added. Bromoacetyl bromide (**2**) diluted with CH_2Cl_2 was then added dropwise to the corresponding aniline mixture using a constant pressure dropping funnel under ice bath conditions. After 2 h, the reaction was completed and quenched with water under TLC monitoring. The mixture was extracted with CH_2Cl_2 (100 mL × 3) and the organic phases were combined. The combined organic phase was washed with saturated aqueous NaCl solution (100 mL) and dried over anhydrous Na_2SO_4. The organic layer was removed under vacuum to obtain the crude product. The crude product was recrystallized to gain the compounds (**3a-g**) with 88–92% yields. (II) Preparation of compounds (6a-v): To a 500 mL round-bottomed flask equipped with a magnetic stirrer, a solution of various substituted benzaldehydes **4a-v** (10 mmol, 1.0 equiv) in ethanol (150 mL) was added. Under stirring, ethyl cyanoacetate **5** (10 mmol, 1.0 equiv), thiourea (10 mmol, 1.0 equiv), and potassium carbonate (10 mmol, 1.0 equiv) were sequentially introduced. The reaction mixture was refluxed for approximately 10–14 h. TLC was used to monitor the progress of the reaction and it showed the starting material was completely consumed. The reaction was cooled to room temperature, then the solids were filtered and washed with EtOH. The solids were dissolved in 200 mL of water at 80 °C and the pH of the solution was adjusted to 5–6 to give the desired white or yellow crude product. The desired crude product was filtered, and recrystallized or purified by silica gel chromatography to gain the 5-cyano-6-arylpyrimidinone derivatives (**6a-v**) with 38–75% yields. (III)

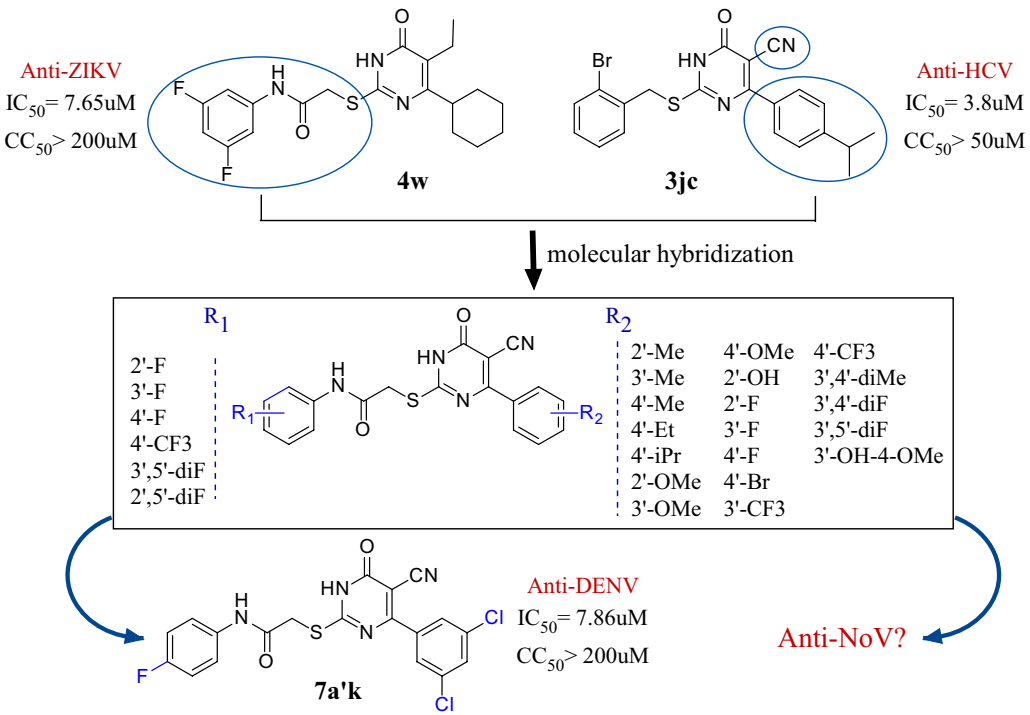

Fig. 1 Target compounds design

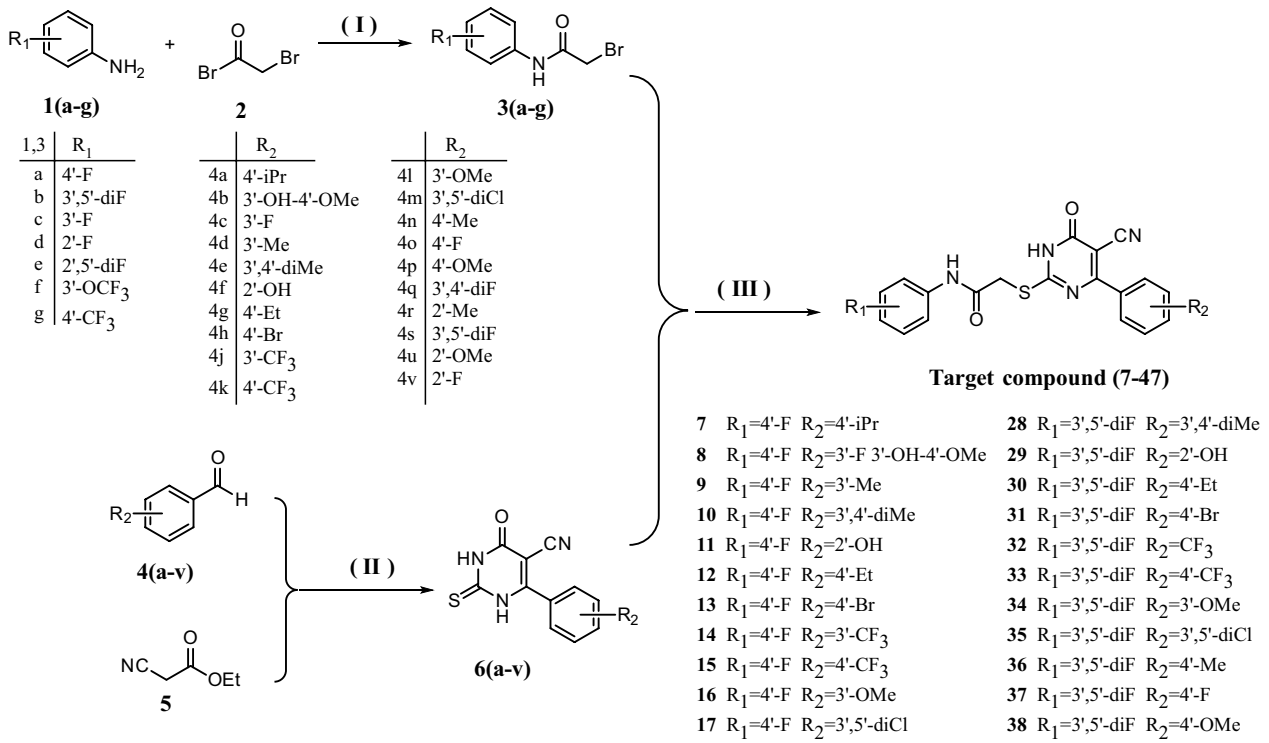

1,3	R_1
a	4'-F
b	3',5'-diF
c	3'-F
d	2'-F
e	2',5'-diF
f	3'-OCF_3
g	4'-CF_3

	R_2
4a	4'-iPr
4b	3'-OH-4'-OMe
4c	3'-F
4d	3'-Me
4e	3',4'-diMe
4f	2'-OH
4g	4'-Et
4h	4'-Br
4j	3'-CF_3
4k	4'-CF_3

	R_2
4l	3'-OMe
4m	3',5'-diCl
4n	4'-Me
4o	4'-F
4p	4'-OMe
4q	3',4'-diF
4r	2'-Me
4s	3',5'-diF
4u	2'-OMe
4v	2'-F

Scheme 1 Synthesis of target compounds. Reagents and reaction conditions: (I) TEA, 0 °C, CH_2Cl_2, 2 h; (II) K_2CO_3, thiourea, EtOH. reflux, 10–14 h; (III) K_2CO_3, DMF, RT

Preparation of target molecules (7–47): The compound **6a-v** (1 mmol, 1 equiv) obtained in the previous step and K_2CO_3 (1.2 mmol, 1.2 equiv) were placed in a round-bottomed flask and dissolved completely in dimethylformamide (20 mL). After stirring the mixture for 30 min, the corresponding compound **3a-g** (1 mmol, 1 equivalent) was added. The reaction was monitored by TLC after 30 min to ensure completion. The reaction was stopped, and the reaction mixture was extracted with ethyl acetate (80 mL × 3). The combined organic phase was washed with saturated NaCl solution (100 mL) and dried over anhydrous Na_2SO_4. The organic layer was removed under vacuum to obtain the crude product. The crude product was recrystallized or purified by silica gel chromatography to gain the target compounds (**7–47**) with 21–92% yields.

41 target compounds were synthesized, and their melting points were determined on a WRS-1 digital melting point apparatus and were calibrated. ^{1}HNMR and ^{13}C NMR spectra were obtained on a Brucker AM 400 MHz spectrometer in the indicated solvents. Chemical shifts are expressed in δ units using Tetramethylsilane (TMS) as an internal reference. Mass spectra were taken on an Agilent LC/MSD TOF mass spectrometer. Solvents were reagent quality and, when necessary, were purified and dried by typical methods. Concentration of the reaction solutions involved the use of rotary evaporator (Heidolph) at reduced pressure. The physical and spectral data of the compounds are listed in Supplementary Tables 1 and Table 2.

The compounds were dissolved in 100% Dimethyl sulfoxide (DMSO) at a concentration of 40 μg/mL, stored at −20 °C, and thawed immediately before use. 2CMC was purchased from MedChemExpress (HY-10468, MCE).

The purity was more than 95% for all compounds that were evaluated in the following experiments.

Cell lines and viruses

293T cells (human embryonic kidney cells, ATCC #CRL-3216), RAW264.7 cells (mouse mononuclear macrophages cells, ATCC #TIB-71), and BV2 cells (mouse microglia cells, RRID #CVCL_0182) were acquired from the Dr. Herbert W. Virgin Laboratory (Washington University School of Medicine in St. Louis). RAW264.7 cells were cultured in MEM media (E2105, EvaCell) with 10% FBS (E01010, EvaCell; BS-1105, OPCEL). BV2 cells and 293 T cells were cultured in DMEM (E2102, EvaCell) with 10% FBS.

Stocks of MNV strains CW3 (MNV^{CW3}, GenBank accession No. EF014462.1) and CR6 (MNV^{CR6}, GenBank accession No. JQ237823) were generated from molecular clones as previously described [38]. Briefly, plasmids encoding viral genomes were transfected into 293 T cells to generate P0 infectious virus following with two passages on BV2 cells to liberate P2 virions. P2 stocks were aliquoted and stored at −80 °C. Titers of virus stocks were determined by three independent plaque assays on RAW264.7 cells prior to use.

Cell viability-based anti-MNV screening

BV2 cells were plated at a density of 10,000 cells/well in black 96-well microplates 16–18 h before infection. Cells were then infected with MNV^{CW3} or MNV^{CR6} at a MOI (multiplicity of infection) of 0.25 followed by cell culture media replacement with 40 μg/mL of the indicated compounds or only DMSO as the vehicle control for 24 h (MNV^{CW3}) or 36 h (MNV^{CR6}). Cell viability was then determined by measuring ATP levels using the CellTiter-Lumi™ luminescence cell viability assay kit according to the manufacturer's instruction (C0065, Beyotime Bio).

MNV plaque assays

MNV infected cells were harvested at 24 h post infection (hpi) and frozen at −80 °C. RAW264.7 cells were seeded at 1.8×10^6 cells/well in 6-well plates. 16 h later, media was removed and tenfold serial dilutions of cell lysate was applied to each well for 1 h with gentle rocking on a digital rocker at 8 rpm. Viral inoculum was then aspirated and 2 mL of overlay media was added (MEM, 10% FBS, 2 mM L-Glutamine, 10 mM HEPES, and 1% methylcellulose). Plates were incubated for 2 days prior to visualization with crystal violet solution (0.2% crystal violet and 20% ethanol).

MNV RNA extraction and viral genome copies quantification

Reverse transcription quantitative PCR (RT-qPCR) was performed to measure the number of MNV genome copies. RNA was extracted from infected cells using a Viral RNA Kit (R1074-02, OMEGA) according to the manufacturer's protocol. 1 μg total RNA was used as a template for cDNA synthesis with the NVoScript®Plus All-in-one 1st Strand cDNA Synthesis system (E047, Novoprotein). MNV TaqMan assays were performed with TaqMan™ Fast Advanced Master Mix (4,444,557, Applied Biosystems), using a standard curve for determination of absolute viral genome copies as previously described [39]. Primers used were: Forward primer CACGCCACC GATCTGTTCTG, Reverse primer GCGCTGCGCCAT CACTC, MGB probe 6FAM-CGCTTTGGAACAATG-MGBNFQ. Copy number was determined by comparing Ct values to a standard curve generated by dilution of a gBlock (IDT) encoding the target sequence.

Expression and purification of MNV and HNV RdRp

The gene of MNV^{CW3} RdRp was inserted into the pET-42a (+) vector and transformed into BL21 (DE3) *E. coli*. Protein was induced at an O.D. 600 of 0.6 with 1 mM IPTG and incubated at 37 °C for 5 h. Afterwards, bacterial pellets were harvested, and lysed with lysozyme and TieChui™ *E. coli* Lysis Buffer (BR00005-01, ACE Bio), followed by centrifugation at 9,000g for 15 min at 4 °C to separate the lysate. MNV^{CW3} RdRp protein was then purified using the BeyoGold™ GST-tag Purification kit (P2251, Beyotime Bio) according to the manufacturer's instructions. Finally, the concentration of protein was quantified using the BCA Protein Assay kit (20201ES86, Yeasen), and the purity of the RdRp was assessed through SDS-PAGE analysis.

The HNV RdRp sequence (G II 0.4/Sydney/2006, GenBank accession No. DQ078829) [40] was synthesized and inserted into the pET-21a (+) vector (General Biol). The protein expression procedure was the same as for MNV^{CW3} RdRp. HNV RdRp protein was purified using the BeyoGold™ His-tag Purification kit (P2226, Beyotime Bio) according to the manufacturer's instructions.

RdRp inhibition assay

Polymerase activity was measured by the detection of the formation of double-stranded RNA (dsRNA) synthesis from poly(C), utilizing the fluorescent dye PicoGreen [41]. RdRp assays were performed as previously described [42]. Black 96-well plates were used to protect the reaction mixture from light. Specifically, in vitro RNA synthesis assays utilized single-stranded RNA poly(C) as a template and GTP as a substrate in a 100 μL reaction volume. 8 μL aliquot of MNV RdRp (35 μM), or HNV RdRp

(35 μM) prepared in reaction buffer (10 mM PBS, pH7.5, 2.5 mM $MnCl_2$, 5 mM DTT), was first incubated with either 4 μL of 100 μM compound or a serial concentration of compound (0–500 μM, when IC_{50} was performed) at 30 °C for 10 min. This was followed by the addition of 4 μL of 1 mg/mL poly(C) (P4903, Sigma-Aldrich) and 4 μL of 625 μM GTP (G452636, Aladdin) to the mixture, and further incubation for 30 min at 30 °C. The final reaction system contains 2.8 μM MNV RdRp, or HNV RdRp, 40 μg/mL poly(C) and 25 μM GTP, along with 4 μM Co-29. The reaction was halted by adding 10 mM EDTA. For detection, 100 μL of PicoGreen dye (P7581, Invitrogen) pre-diluted 200-fold in TE buffer (10mM Tris–HCl, 1mM EDTA, pH7.5) was introduced into each well and incubated for 5 min at room temperature. Quantitative assessment of double-stranded RNA was then performed using a microplate reader at standard wavelengths (excitation 480 nm, emission 520 nm).

Size-exclusion chromatography (SEC) was used to detect the effect of Co-29 on RdRp protein dimer formation. The experiment was carried out with RdRp protein with or without Co-29 as mixtures on a Superose 6 10/300 GL column (GE Healthcare) pre-equilibrated with a buffer containing 20 mM Tris–HCl (pH 8.0), and 150 mM NaCl. The compound concentration was 60 μM. Liquid flow rate used was 0.4 mL/min.

Molecular docking

ChemDraw 20.0 was used to draw the structural formula of the compound, which was then saved in sdf format. Next, Chem3D 20.0 was used to open the structural formula drawn in the previous step to optimize the mechanical structure (click Calculations to select MM2, then continue to select Minimize Energy and the parameters are default, click Run, finally save the result as a mol2 format). The crystal structures of MNV^{CW3} RdRp (PDB ID: 4NRU) and HNV RdRp (PDB ID: 4LQ3) were acquired from the RCSB Protein Data Bank. Molecular docking of Co-29 and RdRp was performed using AutoDock4. Co-29 and RdRp were converted from their native formats into pdbqt formats with AutoDockTools 1.5.7. The structures were optimized by deleting water molecules, removing organic, and adding hydrogen atoms. Then the molecular docking was performed using AutoDockTools 1.5.7. The Lamarckian genetic algorithm was selected as the docking algorithm and select 10 docking times. All docking run options were default values. Finally, the docking results with the highest scores were visualized by PyMoL [43]. The diagram for proteins and Co-29 interaction was generated by the LIGPLOT program [44].

Statistical analysis

All experiments were performed with ≥ 3 biological repeats. Data were analyzed with GraphPad Prism 8 software, expressed as Mean ± SD. In all graphs, four asterisks indicate a P value of < 0.0001, three asterisks indicate a P value of < 0.001, two asterisks indicate a P value of < 0.01, one asterisk indicates a P value of < 0.05, and ns indicates not significant ($P > 0.05$) as determined by Mann Whitney test when comparing two groups, or one-way ANOVA with Tukey's multiple comparisons test when comparing three or more groups.

Results

Cell viability-based anti-MNV compounds screening

Following the procedure described previously [35, 45], 41 5-cyano-2-thiacetoaryl pyrimidinone compounds were synthesized by the molecular hybridization method as illustrated in Scheme 1. These compounds were characterized by ^1H NMR and HRMS for their structural accuracy.

MNV replicates and induces cell death in murine macrophage-like cells, including the microglial BV2 cell line. BV2 cells were infected with MNV^{CW3} for 1 h, and then treated with 40 μg/mL of the synthesized compounds individually. The ratio of live cells (i.e. cell viability) was measured after 24 h incubation. Addition of 40/41 of the compounds tested did not result in increased live cell number. Only one of them, Co-29, exhibited a significantly increased cell viability of 36.9%, compared to the negative control (DMSO only) of about 2.7% (Supplementary Fig. 1A), indicating a preliminary anti-MNV activity of Co-29.

Co-29 inhibits MNV^{CW3} replication in cell culture

We further validated the anti- MNV^{CW3} activity of Co-29 in cell culture. During the screening, only 40 μg/mL of each compound was used for convenience. We then examined the concentration effect of the antiviral activity of Co-29. We found that Co-29 showed significant antiviral activity in BV2 cells after MNV^{CW3} infection at a concentration from 30 to 60 μg/mL (Fig. 2A). The lower cell viability at 60 and 70 μg/mL might be resultant from the cytotoxicity of this compound, since the CC_{50} of Co-29 in BV2 cells was about 52.20 μg/mL (126 μM) (Supplementary Fig. 1B). We next treated MNV^{CW3} infected BV2 cells with 40 μg/mL (97 μM) of Co-29 to examine the inhibition of viral replication. By quantification of the viral genome copies after 24 h treatment, the RNA level of MNV^{CW3} was more than 2 Log_{10}-fold decreased in the Co-29 treated group than in the DMSO vehicle control group (Fig. 2B), with an EC_{50} value of 58.22 μM (Fig. 2D), which was well below the CC_{50} value (126 μM). Plaque assays were also used to detect the antiviral activity of

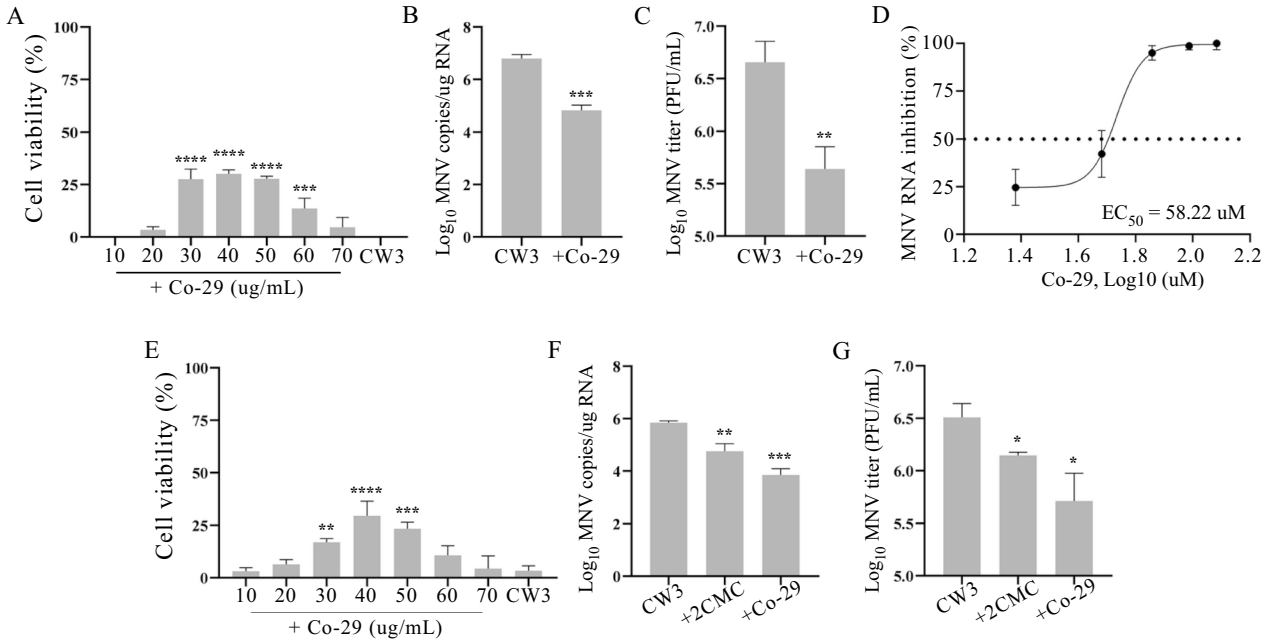

Fig. 2 Co-29 inhibits MNV^{CW3} replication in cell culture. **A** The ratio of live BV2 cells with Co-29 treatment at different concentrations after MNV^{CW3} infection for 24 h. **B** The viral RNA levels in BV2 cells with or without 97 μM (40 μg/mL) Co-29 treatment after MNV^{CW3} infection for 24 h. **C** The viral titers in BV2 cells with or without 97 μM Co-29 treatment after MNV^{CW3} infection for 24 h. **D** EC_{50} value of Co-29 by viral RNA levels in BV2 cells infected by MNV^{CW3}. **E** The ratio of live RAW264.7 cells with Co-29 treatment at different concentrations after MNV^{CW3} infection for 24 h. **F** The viral RNA levels in RAW264.7 cells with 40 μg/mL 2CMC or Co-29 treatment after MNV^{CW3} infection for 24 h. **G** The viral titers in RAW264.7 cells with 40 μg/mL 2CMC or Co-29 treatment after MNV^{CW3} infection for 24 h. Data are shown as Mean ± SD. n ≥ 3. *$P < 0.05$, **$P < 0.01$, ***$P < 0.001$, ****$P < 0.0001$

Co-29. As shown in Fig. 2C, Co-29 dramatically inhibited the formation of MNV^{CW3} plaques, reflecting the viral titer.

To re-verify the inhibitory effect of Co-29 on MNV at the molecular level, we used another commonly used cell line for in vitro MNV infection, the macrophage-like cell line RAW264.7 [46]. Similar as seen in the BV2 cells, Co-29 showed significant antiviral activity at a concentration from 30 to 60 μg/mL, with a maximum effectiveness at 40 μg/mL (Fig. 2E). We used a NA, 2CMC, which has been shown to inhibit HNV [47] and MNV [19] infection, as a positive control to compare its antiviral activity with Co-29's. At the same concentration (40 μg/mL), both 2CMC and Co-29 treatment resulted in decreased MNV^{CW3} genome copy number (Fig. 2F) and viral titers (Fig. 2G), with a trend toward a more inhibitory effect by Co-29 (Fig. 2F, G). Further assessment of the CC_{50} of Co-29 in RAW264.7 cells was 104.9 μM (Supplementary Fig. 1C). Thus, the inhibitory effect of Co-29 on MNV^{CW3} is not dependent on cell type, but rather appears to be viral-specific, indicating the potential of Co-29 as an anti-MNV candidate.

Co-29 inhibits MNV^{CR6} replication in cell culture

MNV^{CR6} is another wildly used strain which causes persistent enteric infection in mice [48]. We then examined if Co-29 also shows antiviral activity in BV2 cells infected by MNV^{CR6}. Similar to the MNV^{CW3} results, Co-29 exhibited inhibition of MNV^{CR6} replication in BV2 and RAW264.7 cells, accompanied with increased cell viability (Fig. 3A, D), low levels of viral genome copies (Fig. 3B, E), and decreased plaque numbers (Fig. 3C, F). These results indicate the potential for a broad anti-MNV activity of Co-29.

Co-29 inhibits norovirus RdRp activity

Based on the strategy to synthesize the serial compounds in this study, we hypothesized that Co-29 may have a direct inhibitory effect on the activity of MNV RdRp. To explore this hypothesis, we expressed and purified RdRp of MNV^{CW3} in *E. coli*. The purity of the protein was assessed by Commassie brilliant blue staining of SDS-PAGE gels (Supplementary Fig. 2A, B) and size-exclusion chromatography (SEC) (Supplementary Fig. 2C, D). We then evaluated the inhibitory activity of Co-29 against MNV RdRp by an in vitro fluorescent de novo RdRp assay [42]. Co-29 was tested and compared to mock treated samples containing vehicle only (0.5%

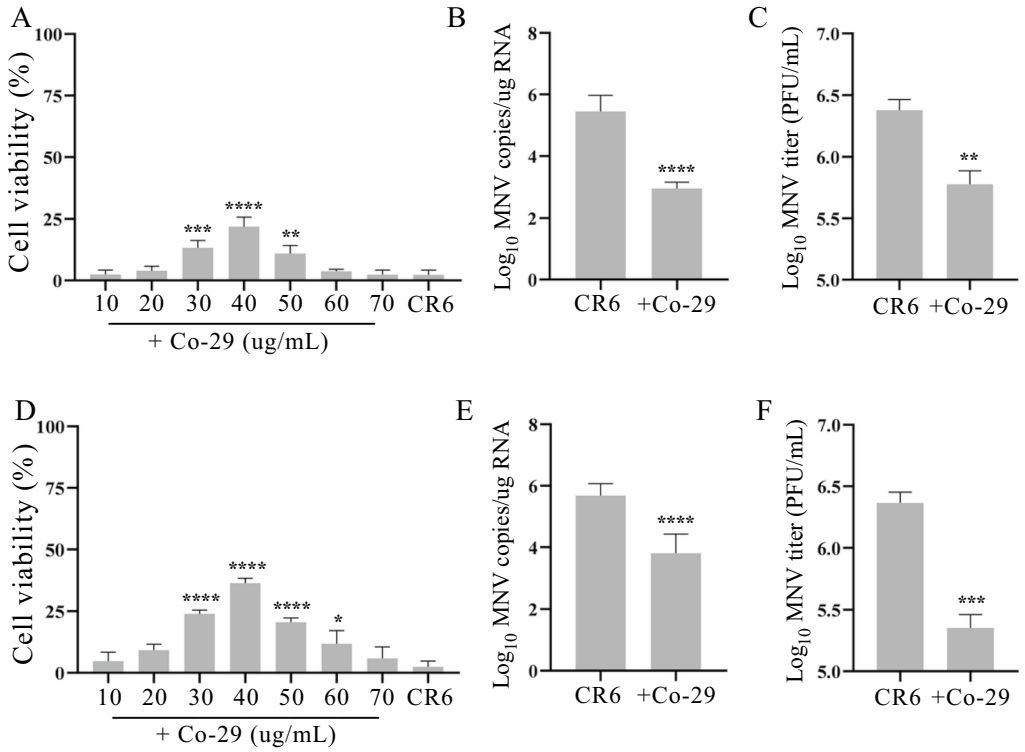

Fig. 3 Co-29 inhibits MNV^{CR6} replication in cell culture. **A** The ratio of live BV2 cells with Co-29 treatment at different concentrations after MNV^{CR6} infection for 24 h. **B** The viral RNA levels in BV2 cells with or without 97 μM (40 μg/mL) Co-29 treatment after MNV^{CR6} infection for 24 h. **C** The viral titers in BV2 cells with or without 97 μM Co-29 treatment after MNV^{CR6} infection for 24 h. **D** The ratio of live RAW264.7 cells with Co-29 treatment at different concentrations after MNV^{CR6} infection for 24 h. **E** The viral RNA levels in RAW264.7 cells with or without 97 μM Co-29 treatment after MNV^{CR6} infection for 24 h. **F** The viral titers in RAW264.7 cells with or without 97 μM Co-29 treatment after MNV^{CR6} infection for 24 h. Data are shown as Mean ± SD. n ≥ 3. *P < 0.05, **P < 0.01, ***P < 0.001, ****P < 0.0001

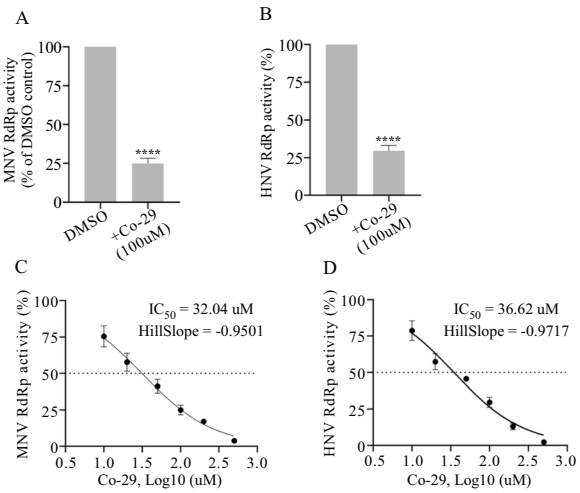

Fig. 4 Co-29 inhibits the enzyme activity of MNV^{CW3} RdRp and HNV RdRp. **A** The inhibition of MNV^{CW3} RdRp activity by Co-29. **B** The inhibition of HNV RdRp activity by Co-29. Percentage of inhibition was normalized to the DMSO vehicle control group. **C** IC_{50} value of Co-29 to inhibit MNV^{CW3} RdRp activity. **D** IC_{50} value of Co-29 to inhibit HNV RdRp activity. Data are shown as Mean ± SD. n ≥ 3. ****P < 0.0001

DMSO). Using this assay, Co-29 showed more than a 75% inhibition of MNV^{CW3} RdRp with 35 μM RdRp in the reaction system (Fig. 4A). To further evaluate the effect of Co-29 against HNV RdRp, we detected the inhibitory activity of Co-29 on HNV RdRp with the same assay. As shown in Fig. 4B, Co-29 exhibited more than 70% inhibition of HNV RdRp. As well, Co-29 inhibited the activity of MNV^{CW3} RdRp and HNV RdRp in a dose-dependent manner, with an IC_{50} value of 32.04 μM for MNV RdRp (Fig. 4C), and 36.62 μM for HNV RdRp (Fig. 4D), respectively. To exclude the possible aggregative inhibition effect by Co-29 on RdRp protein aggregates formation, SEC was performed using MNV RdRp and HNV RdRp with or without Co-29. Chromatograms showed that the main peak formed by the protein did not change when Co-29 was added to the mixture (Supplementary Fig. 2E, F), indicating no enzyme aggregative inhibition effect in the RdRp inhibition system we used. In conclusion, these results indicate that Co-29 has a potential broad-spectrum activity against norovirus RdRp.

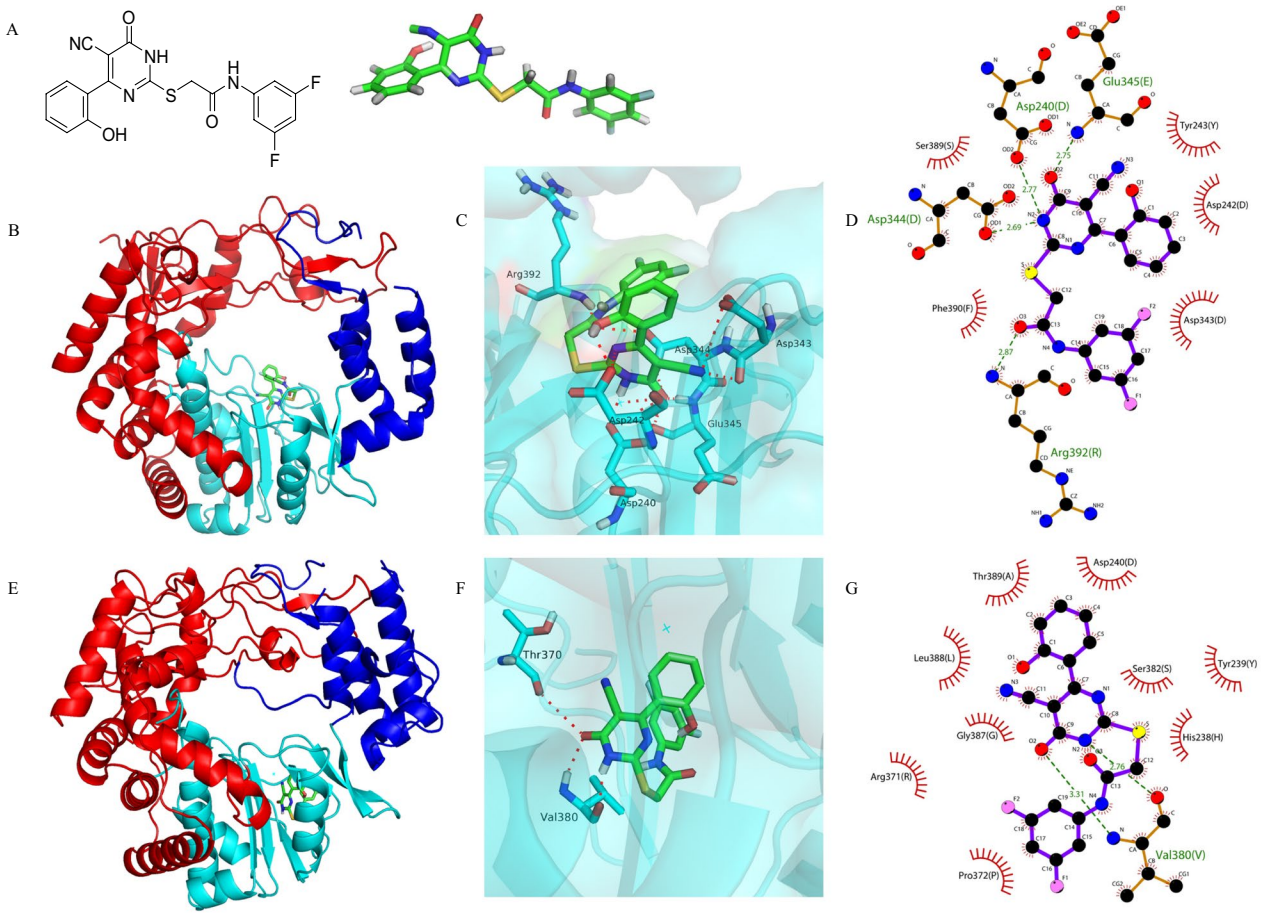

Fig. 5 Predicted binding sites for Co-29 in MNV and HNV RdRp. **A** Chemical structure of Co-29 (left: 2D; right: 3D, color indication: green for carbon, red for oxygen, grey for hydrogen, yellow for sulphur, dark blue for nitrogen, and light blue for fluorine). **B**, **E** Predicted structure of MNV^{CW3} RdRp (PDB:4NRU) (**B**) or HNV RdRp (PDB:4LQ3) (**E**) in complex with Co-29. Co-29 is shown as green mesh. RdRp domains are color-coded: fingers (red), palm (cyan), thumb (blue). **C**, **F** The magnified three-dimensional structure of the interaction between Co-29 and MNV^{CW3} RdRp (**C**) or HNV RdRp (**F**). Co-29 and the amino acid residues involved the interactions are shown as red dashed line. **D**, **G** Schematic representation of the interactions between Co-29 and MNV^{CW3} RdRp (**D**) or HNV RdRp (**G**) as calculated by LIGPLOT

The predicted interaction of Co-29 with norovirus RdRp

Norovirus RdRp possesses three major domains termed the thumb, fingers, and palm [15, 16]. To better understand the interaction of Co-29 with norovirus RdRp, we conducted a molecular docking assessment to predict the binding mode of MNV RdRp and HNV RdRp in complex with Co-29. The structure of Co-29 is depicted in Fig. 5A. Using the AutoDock program, we first docked Co-29 into the crystal structure of MNV RdRp in complex with the inhibitor Compound 6 (a Suramin derivative) (PDB ID: 4NRU) [49]. As shown in Fig. 5B, the binding pocket of Co-29 locates in the palm subdomain of MNV RdRp (Fig. 5B), and preferentially binds to amino acids Asp240, Asp242, Asp343, Asp344, Glu345, and Arg392 at the active site (Fig. 5C), with a binding energy of − 7.29 kcal/mol. A schematic diagram of these interactions was generated by using LIGPLOT [44]. Four hydrogen bonding interactions occur between Co-29 and MNV RdRp (Fig. 5D). The first is the one between Arg392 of MNV RdRp and the carbonyl group on the *C*-2 thioacetyl phenyl amine side chain. In addition, Asp240, Asp344, and Glu345 forms three hydrogen bonds with the pyrimidine ring of Co-29. Further, we put Co-29 with Compound 6 or PPNDS (PDB ID: 4O4R) [29] separately into the MNV RdRp structure to compare their interaction locations and found no overlap between each group (Supplementary Fig. 3A, B), indicating a novel interaction between Co-29 and MNV RdRp other than occupying either the NNI binding A site and B site in norovirus RdRp.

In addition to exploring the interaction between the compound and MNV RdRp, we also predicted whether Co-29 binds to HNV RdRp. Using the same method, we docked Co-29 to the crystal structure of HNV RdRp in

complex with inhibitor PPNDS (PDB ID: 4LQ3) [26]. The binding pocket of Co-29 locates into the palm subdomain of HNV RdRp (Fig. 5E). The main amino acids contributing to the interaction in the binding cavity are Thr370 and Val380 (Fig. 5F). Val380 forms two hydrogen bonds with the pyrimidine ring of Co-29 at different sites (Fig. 5G). The binding energy of Co-29 with HNV RdRp is −5.99 kcal/mol, slightly higher than the binding energy with MNV RdRp (−7.29 kcal/mol). This energy difference was mainly due to less hydrogen bonds between Co-29 and HNV RdRp, preventing their effective interaction. Additionally, there exists no overlap between the interaction locations of Co-29 and PPNDS with HNV RdRp (Supplementary Fig. 3C).

To evaluate the effectivity of Co-29 as a potential broad-spectrum compound against norovirus viral infection and RdRp activity, we aligned multiple sequences of RdRp from different viral genotypes from mouse and human (Supplementary Table 3). We then analysed the conservation of binding sites of Co-29 with RdRp across these norovirus variants, and found the Co-29-interacting residues in MNV RdRp were highly conserved in all analysed sequences (Fig. 6). The HNV GII.4 genotype has long been the predominant cause of gastroenteritis outbreaks globally, being renowned for its high infectivity and capacity to cause large-scale outbreaks [50]. The Co-29-interacting residue Val380 of HNV RdRp in the GII variants GII.4/Sydney/2006 and GII.4/Sydney/2012 [40, 51] were conserved (Fig. 6). These results suggest that Co-29 may be a general inhibitor of norovirus RdRp.

Discussion

Norovirus has been circulating in the human population for more than 50 years [52]. Ever since its discovery, norovirus has been recognised as a significant etiological agent of acute gastroenteritis. In recent years, the incidence of acute gastroenteritis associated with norovirus has been steadily increasing, causing both a clinical and economic burden [4, 8]. GII.4 is the predominant genotype of HNV. With successive accumulation of mutations on VP1, which causes a shift in antigenic properties, facilitating variants escape from the immune system [53]. In the past few years, the GII.17 variant has led to numerous outbreaks, including in developed countries [4, 54]. As well as VP1, RdRp contains a variable motif, contributing to the genetic and antigenic diversity of HNV [55]. Due to the extreme infectivity, genetic diversity, and rapid evolution, norovirus possesses the ability to pose a serious threat to human health while hindering the development of effective vaccines or antiviral drugs.

While there is a growing interest in developing antiviral drugs for norovirus, treatments remain limited, and prevention through hygiene is still the primary strategy for managing norovirus outbreaks. RdRp is the critical and highly conserved enzyme for viral genome synthesis among different norovirus strains and even across RNA viruses, which endows it as an ideal antiviral drug target. Also because of this reason, antiviral compounds developed against other RNA viruses have been commonly examined for repurposing as norovirus therapeutics [34]. For example, the wildly studied anti-norovirus agent 2CMC was originally developed against HCV, but it also exhibited in vitro activity against other flaviviruses, including DENV[56]. A study evaluating the antiviral activity of six HCV NNIs against the HNV RdRp found that JTK-109 had antiviral activity across several genera of *Caliciviridae* with a low IC_{50} value for HNV RdRp and EC_{50} for MNV replication [28]. Recently, a group performed a structure-based virtual screening taking advantage of the structurally equivalent site in DENV and HNV RdRp, identifying RAI-13 as a potent inhibitor to both HNV and DENV infection [27]. In recent years, our group have launched the strategy of design and synthesis of a new series of scaffolds based on the core structure of compounds with good anti-HCV or -HIV activity to acquire novel compounds against other RNA viruses such as ZIKV and DENV [37, 57]. The series of novel 5-cyano-2-thiacetyl aromatic pyrimidinone target compounds used in this study were synthesized with a skeleton bearing common structure of anti-HCV and anti-ZIKV drugs [37]. With a similar design strategy, one newly synthesized compound has been shown to inhibit DENV RdRp enzyme activity [35], indicating the feasibility and effectiveness of this repurposing antiviral strategy to develop new drug candidates for norovirus infection.

In this study, we synthesized a compound library with 41 5-cyano-2-thiacetyl aromatic pyrimidinones using molecular hybridization method with 3jc, a HCV RdRp inhibitor [36], and 4w, a ZIKV RdRp inhibitor [37] as the lead compounds. We then performed a screening with MNV in vitro infection in cell culture system to find hit targets showing antiviral activity. Since the discovery of MNV, it has been used as a powerful in vitro and in vivo model for norovirus studies [58]. MNV replicates and induces cell death in murine macrophage-like cells, including the microglial BV2 cell line and RAW264.7 cells. This fact allows for the in vitro cell viability-based screening of compounds which exhibit anti-MNV activity, resulting in an increased ratio of live cells. One of the compounds, Co-29, was identified as a potential target. Co-29 treatment effectively inhibits MNV RNA

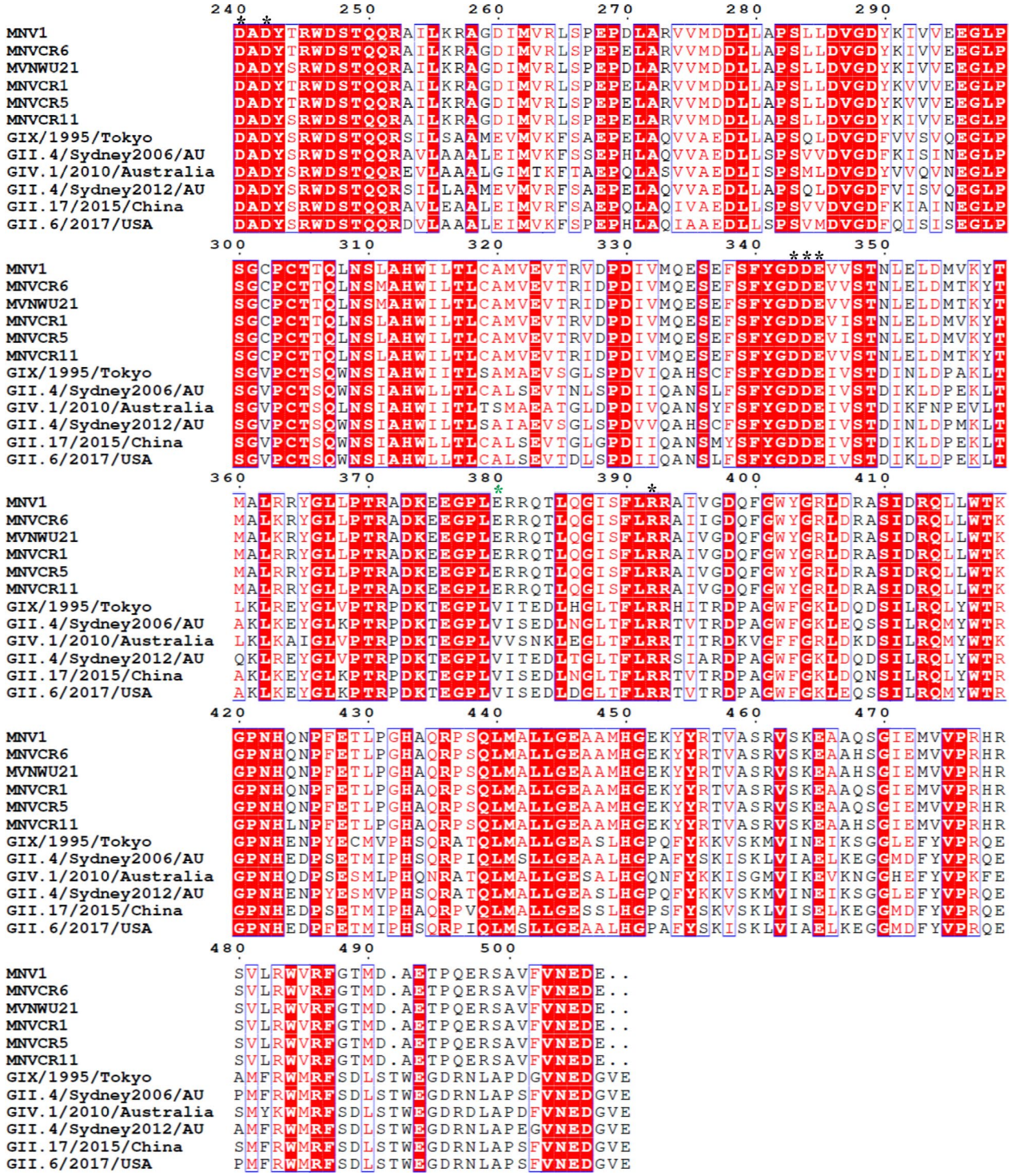

Fig. 6 Sequence alignment of 10 norovirus RdRp proteins. Sequence alignment of RdRps from MNV (MNV1, MNVCR6, MNVWU21, MNVCR1, MNVCR5), HNV GII.4 (GII.4/Sydney/2006, GII.4/Sydney/2012), HNV GII.6 (HuGII.6), HNV GII.17 (GII.17/CHN/2015) and HNV GIX. Black asterisks mark the residues in MNV^{CW3} RdRp (PDB:4NRU) interacting with Co-29 by hydrogen bonds; green asterisk marks the residues in HNV RdRp (PDB:4LQ3) interacting with Co-29 by hydrogen bonds

replication (EC_{50} = 58.22 μM) and viral proliferation, leading to significantly increased live-cell number using two MNV strains in two different cell lines. An RdRp enzyme activity assay indicated that Co-29 directly inhibits the enzyme activity of both MNV RdRp (IC_{50} = 32.04 μM) and HNV RdRp (IC_{50} = 36.62 μM). Molecular docking prediction suggested that Co-29 interaction with the active sites of RdRp via specific residues, which are different from the known compound-binding sites previously reported. Furthermore, the predicted binding sites of Co-29 are highly conserved across the various MNV and HNV strains, indicating the broad-spectrum antiviral activity of Co-29 against norovirus.

Great efforts have been put on anti-norovirus drug identification through different screening strategies. Structure-based virtual screening or cell-free inhibition of RdRp enzyme activity are frequently used approaches in previous studies [34]. A big limitation to these methods is the effectivity of the identified potential drugs in living cells or animals. We performed the screening in cell culture by detecting the live cell ratio after MNV in vitro infection. Therefore, we could monitor the cell viability to estimate the antiviral effect of the screened compounds, since almost 100% infected cells would die by infection with a certain amount of virus at the indicated time. By utilizing this cell-based assay we were able to identify authentic antivirals, excluding possible artificial results, resulting in compound discovery with a higher potential for in vivo therapeutics.

It should also be noted that although Co-29 treatment resulted in significant decreased MNV RNA copy number and low viral titer compared to vehicle control or even 2CMC treatment, the EC_{50} or IC_{50} values of Co-29 are still high to a certain extent, compared to the other antiviral compounds identified from previous studies [34, 59]. Therefore, further structure-based optimization of Co-29 is needed to improve the efficiency against norovirus RdRp and reduce the cytotoxicity to develop more potent inhibitors. Also, an in vivo mouse infection model is needed to be developed to prove a platform to assess the potential of anti-norovirus compounds, including Co-29, or structure-optimized compounds based on Co-29.

Conclusions

In conclusion, our study suggests that the newly synthesized Co-29 may serve as a potential antiviral agent in the management of norovirus infections.

Abbreviations

CC_{50}	Concentration of 50% cytotoxicity
DENV	Dengue virus
EC_{50}	Concentration for 50% of maximal effect
FBS	Fetal bovine serum
FDA	Food and drug administration
HCV	Hepatitis C virus
HIV	Human immunodeficiency virus
HNV	Human norovirus
hpi	Hours post-infection
IC_{50}	Half maximal inhibitory concentration
MNV	Murine norovirus
MOI	Multiplicity of infection
ORFs	Open reading frames
PFU	Plaque forming unit
RdRp	RNA-dependent RNA polymerase
SEC	Size-exclusion chromatography
ZIKV	Zika virus
2CMC	2′-C-methylcytidine

Supplementary Information

The online version contains supplementary material available at https://doi.org/10.1186/s12985-025-02687-w.

Additional file 1

Author contributions

L.X. and H.J. performed all the biological experiments and analysed the data; W.J. and W.J. synthesized the chemical compounds; T.Y. contributed the anti-MNV screening; W.C. contributed the plasmids construction; C.Q. drew the 2D interaction diagram; L.X., W.C. and W.J. drafted the manuscript; L.K. edited the language and provided scientific criticism; H.Y. and L.Q. wrote and revised the manuscript and supervised this study. All authors read and approved the final manuscript.

Funding

This work was supported by Yunnan Fundamental Research Projects (202301BF070001-014 to L. Q. and 202301AU070202 to W. C.), National Natural Science Foundation of China (32070745 to L. Q.; 82273820 and 21967020 to H. Y.), and the Yunnan University Startup Program (L. Q.).

Availability of data and materials

No datasets were generated or analysed during the current study.

Declarations

Ethics approval and consent to participate

Not applicable.

Consent for publication

Not applicable.

Competing interests

The authors declare no competing interests.

Received: 9 December 2024 Accepted: 28 February 2025
Published online: 04 April 2025

References

1. Lopman BA, et al. The vast and varied global burden of norovirus: prospects for prevention and control. PLoS Med. 2016;13(4):e1001999.
2. Atmar RL, Ramani S, Estes MK. Human noroviruses: recent advances in a 50-year history. Curr Opin Infect Dis. 2018;31(5):422–32.
3. Cortes-Penfield NW, et al. Prospects and challenges in the development of a norovirus vaccine. Clin Ther. 2017;39(8):1537–49.
4. Cohen J. Why the "Ferrari of viruses" is surging. Science. 2025;387(6731):235–6.

5. Pires SM, et al. Aetiology-specific estimates of the global and regional incidence and mortality of diarrhoeal diseases commonly transmitted through food. PLoS ONE. 2015;10(12):e0142927.
6. Zhang Q, et al. Recent insights into reverse genetics of norovirus. Virus Res. 2023;325:199046.
7. de Graaf M, van Beek J, Koopmans MP. Human norovirus transmission and evolution in a changing world. Nat Rev Microbiol. 2016;14(7):421–33.
8. Chen J, et al. Advances in human norovirus research: Vaccines, genotype distribution and antiviral strategies. Virus Res. 2024;350:199486.
9. Karst SM, et al. Advances in norovirus biology. Cell Host Microbe. 2014;15(6):668–80.
10. Chhabra P, et al. Updated classification of norovirus genogroups and genotypes. J Gen Virol. 2019;100(10):1393–406.
11. Vongpunsawad S, Venkataram Prasad BV, Estes MK. Norwalk virus minor capsid protein VP2 associates within the VP1 shell domain. J Virol. 2013;87(9):4818–25.
12. Prasad BV, et al. X-ray crystallographic structure of the Norwalk virus capsid. Science. 1999;286(5438):287–90.
13. Thorne LG, Goodfellow IG. Norovirus gene expression and replication. J Gen Virol. 2014;95(Pt 2):278–91.
14. Malet H, et al. The flavivirus polymerase as a target for drug discovery. Antiviral Res. 2008;80(1):23–35.
15. Högbom M, et al. The active form of the norovirus RNA-dependent RNA polymerase is a homodimer with cooperative activity. J Gen Virol. 2009;90(Pt 2):281–91.
16. Lee JH, et al. Crystal structures of murine norovirus-1 RNA-dependent RNA polymerase. J Gen Virol. 2011;92(Pt 7):1607–16.
17. Smertina E, et al. Calicivirus RNA-dependent RNA polymerases: evolution, structure, protein dynamics, and function. Front Microbiol. 2019;10:1280.
18. Galmarini CM, Mackey JR, Dumontet C. Nucleoside analogues: mechanisms of drug resistance and reversal strategies. Leukemia. 2001;15(6):875–90.
19. Rocha-Pereira J, et al. Inhibition of norovirus replication by the nucleoside analogue 2'-C-methylcytidine. Biochem Biophys Res Commun. 2012;427(4):796–800.
20. Rocha-Pereira J, et al. The viral polymerase inhibitor 2'-C-methylcytidine inhibits Norwalk virus replication and protects against norovirus-induced diarrhea and mortality in a mouse model. J Virol. 2013;87(21):11798–805.
21. Costantini VP, et al. Antiviral activity of nucleoside analogues against norovirus. Antivir Ther. 2012;17(6):981–91.
22. Rocha-Pereira J, Jochmans D, Neyts J. Prophylactic treatment with the nucleoside analogue 2'-C-methylcytidine completely prevents transmission of norovirus. J Antimicrob Chemother. 2015;70(1):190–7.
23. Caillet-Saguy C, Simister PC, Bressanelli S. An objective assessment of conformational variability in complexes of hepatitis C virus polymerase with non-nucleoside inhibitors. J Mol Biol. 2011;414(3):370–84.
24. Giancotti G, et al. Structural investigations on novel non-nucleoside inhibitors of human norovirus polymerase. Viruses. 2022;15(1):74.
25. Mastrangelo E, et al. Structure-based inhibition of Norovirus RNA-dependent RNA polymerases. J Mol Biol. 2012;419(3–4):198–210.
26. Tarantino D, et al. Naphthalene-sulfonate inhibitors of human norovirus RNA-dependent RNA-polymerase. Antiviral Res. 2014;102:23–8.
27. Yi D, et al. Identification of a broad-spectrum viral inhibitor targeting a novel allosteric site in the RNA-Dependent RNA polymerases of dengue virus and norovirus. Front Microbiol. 2020;11:1440.
28. Netzler NE, et al. Broad-spectrum non-nucleoside inhibitors for caliciviruses. Antiviral Res. 2017;146:65–75.
29. Croci R, et al. PPNDS inhibits murine Norovirus RNA-dependent RNA-polymerase mimicking two RNA stacking bases. FEBS Lett. 2014;588(9):1720–5.
30. Ferla S, et al. In silico screening for human norovirus antivirals reveals a novel non-nucleoside inhibitor of the viral polymerase. Sci Rep. 2018;8(1):4129.
31. Liu Y, et al. CX-6258 hydrochloride hydrate: a potential non-nucleoside inhibitor targeting the RNA-dependent RNA polymerase of norovirus. Virology. 2024;595:110088.
32. Srinivasan A, et al. Identification and characterization of human apurinic/apyrimidinic endonuclease-1 inhibitors. Biochemistry. 2012;51(31):6246–59.
33. Mastrangelo E, et al. Delivery of suramin as an antiviral agent through liposomal systems. ChemMedChem. 2014;9(5):933–9.
34. Netzler NE, Enosi Tuipulotu D, White PA. Norovirus antivirals: Where are we now? Med Res Rev. 2019;39(3):860–86.
35. Wang JB, et al. Design, synthesis, and activity of 5-cyano-2-thiacetyl aromatic pyrimidinone as DENV NS5 RdRp inhibitors. Acta Pharmac Sin. 2023;58(11):3379–88.
36. Ding Y, et al. Parallel synthesis of 5-cyano-6-aryl-2-thiouracil derivatives as inhibitors for hepatitis C viral NS5B RNA-dependent RNA polymerase. Bioorg Chem. 2006;34(1):26–38.
37. Zhou GF, et al. Identification of 6ω-cyclohexyl-2-(phenylamino carbonylmethylthio)pyrimidin-4(3H)-ones targeting the ZIKV NS5 RNA dependent RNA polymerase. Front Chem. 2022;10:1010547.
38. Lee S, et al. Intestinal antiviral signaling is controlled by autophagy gene Epg5 independent of the microbiota. Autophagy. 2022;18(5):1062–77.
39. Baert L, et al. Detection of murine norovirus 1 by using plaque assay, transfection assay, and real-time reverse transcription-PCR before and after heat exposure. Appl Environ Microbiol. 2008;74(2):543–6.
40. Bull RA, et al. Emergence of a new norovirus genotype II4 variant associated with global outbreaks of gastroenteritis. J Clin Microbiol. 2006;44(2):327–33.
41. Singer VL, et al. Characterization of PicoGreen reagent and development of a fluorescence-based solution assay for double-stranded DNA quantitation. Anal Biochem. 1997;249(2):228–38.
42. Eltahla AA, et al. A fluorescence-based high-throughput screen to identify small compound inhibitors of the genotype 3a hepatitis C virus RNA polymerase. J Biomol Screen. 2013;18(9):1027–34.
43. Schrodinger L. The PyMOL molecular graphics system, Version 1.8 2015.
44. Wallace AC, Laskowski RA, Thornton JM. LIGPLOT: a program to generate schematic diagrams of protein-ligand interactions. Protein Eng. 1995;8(2):127–34.
45. Wu Y, et al. Synthesis and biological evaluation of a series of 2-(((5-akly/aryl-1H-pyrazol-3-yl)methyl)thio)-5-alkyl-6-(cyclohexylmethyl)-pyrimidin-4(3H)-ones as potential HIV-1 inhibitors. Acta Pharm Sin B. 2020;10(3):512–28.
46. Bok K, et al. Apoptosis in murine norovirus-infected RAW264.7 cells is associated with downregulation of survivin. J Virol. 2009;83(8):3647–56.
47. Kolawole AO, et al. Inhibition of human norovirus by a viral polymerase inhibitor in the B cell culture system and in the mouse model. Antiviral Res. 2016;132:46–9.
48. Nice TJ, et al. A single-amino-acid change in murine norovirus NS1/2 is sufficient for colonic tropism and persistence. J Virol. 2013;87(1):327–34.
49. Croci R, et al. Structural bases of norovirus RNA dependent RNA polymerase inhibition by novel suramin-related compounds. PLoS ONE. 2014;9(3):e91765.
50. Hassan E, Baldridge MT. Norovirus encounters in the gut: multifaceted interactions and disease outcomes. Mucosal Immunol. 2019;12(6):1259–67.
51. Lim KL, et al. A multi-site study of norovirus molecular epidemiology in Australia and New Zealand, 2013–2014. PLoS ONE. 2016;11(4):e0145254.
52. Kapikian AZ, et al. Visualization by immune electron microscopy of a 27-nm particle associated with acute infectious nonbacterial gastroenteritis. J Virol. 1972;10(5):1075–81.
53. Kendra JA, et al. Antigenic cartography reveals complexities of genetic determinants that lead to antigenic differences among pandemic GII4 noroviruses. Proc Natl Acad Sci USA. 2021. https://doi.org/10.1073/pnas.2015874118.
54. Gao J, et al. GII.17[P17] and GII.8[P8] noroviruses showed different RdRp activities associated with their epidemic characteristics. J Med Virol. 2023;95(1):e28216.
55. Arias A, et al. Norovirus polymerase fidelity contributes to viral transmission in vivo. mSphere. 2016;1(5).
56. Pierra C, et al. Synthesis and pharmacokinetics of valopicitabine (NM283), an efficient prodrug of the potent anti-HCV agent 2'-C-methylcytidine. J Med Chem. 2006;49(22):6614–20.
57. Rui RM, et al. C6-structural optimizations of 2-aryl-1H-pyrazole-S-DABOs: from anti-HIV to anti-DENV activity. Bioorg Chem. 2022;119:105494.
58. Karst SM, et al. STAT1-dependent innate immunity to a norwalk-like virus. Science. 2003;299:1575–8.
59. Winder N, Gohar S, Muthana M. Norovirus: an overview of virology and preventative measures. Viruses. 2022;14(12):2811.